

Design, Synthesis, and Characterization of Peptide-Based Rab Geranylgeranyl Transferase Inhibitors[†]

Kui-Thong Tan,[‡] Ester Guiu-Rozas,[‡] Robin S. Bon,[‡] Zhong Guo,[§] Christine Delon,[§] Stefan Wetzel,[‡] Sabine Arndt,[‡] Kirill Alexandrov,^{§,||} Herbert Waldmann,[‡] Roger S. Goody,^{§,||} Yao-Wen Wu,[§] and Wulf Blankenfeldt^{*,§}

[‡]Department of Chemical Biology and [§]Department of Physical Biochemistry, Max Planck Institute of Molecular Physiology, Otto-Hahn-Strasse 11, 44227 Dortmund, Germany, and ^{||}Institute for Molecular Bioscience, The University of Queensland, 306 Carmody Road, St. Lucia, QLD 4072, Australia

Received July 28, 2009

Rab geranylgeranyl transferase (RabGGTase) catalyzes the attachment of geranylgeranyl isoprenoids to Rab guanine triphosphatases, which are key regulators in vesicular transport. Because geranylgeranylation is required for proper function and overexpression of Rabs has been observed in various cancers, RabGGTase may be a target for novel therapeutics. The development of selective inhibitors is, however, difficult because two related enzymes involved in other cellular processes exist in eukaryotes and because RabGGTase recognizes protein substrates indirectly, resulting in relaxed specificity. We report the synthesis of a peptidic library based on the farnesyl transferase inhibitor peptidocinnamin E. Of 469 compounds investigated, several were identified as selective for RabGGTase with low micromolar IC₅₀ values. The compounds were not generally cytotoxic and inhibited Rab isoprenylation in COS-7 cells. Crystal structure analysis revealed that selective inhibitors interact with a tunnel unique to RabGGTase, implying that this structural motif is an attractive target for improved RabGGTase inhibitors.

Introduction

Posttranslational modification of proteins with isoprenoids is a crucial process in eukaryotic cells, affecting many proteins involved in signal transduction, cytoskeletal rearrangement, and vesicular transport. Covalent attachment of either a C15 farnesyl or a C20 geranylgeranyl group to conserved C-terminal cysteine residues enables isoprenylated proteins to interact reversibly with intracellular membranes and with other proteins.¹ The majority of proteins undergoing isoprenylation belongs to the Ras superfamily of small guanosine triphosphatases (GTPases), within which the Rab proteins constitute the largest subgroup with over 60 members. The Rab proteins regulate intracellular vesicular transport in eukaryotic cells through association with specific membranes and recruitment of a plethora of Rab-specific effector proteins responsible for budding, transport, tethering/docking, and fusion of vesicles.^{2,3}

Protein isoprenylation is catalyzed by three related enzymes that transfer isoprenyl groups from the corresponding pyrophosphates to their substrate proteins in a reaction involving a Zn²⁺ cation bound to the active center. The isoprenyl transferases can be divided into two categories according to their substrates. On the one hand, the CAAX isoprenyl transferases, protein farnesyl transferase (FTase^a) and protein geranylgeranyl transferase I (GGTase-I), are closely related and

transfer a single isoprenyl group to proteins containing a C-terminal CAAX sequence, including Ras, Rho/Rac, nuclear lamins A and B, heterotrimeric G proteins, and yeast mating factor. Geranylgeranylation of the Rab proteins, on the other hand, is catalyzed by a distinct enzyme termed Rab geranylgeranyl transferase (RabGGTase, GGTase-II). Other than containing typically two cysteines (in some cases one) for attachment of the isoprenoid moieties, the C-termini of Rab proteins do not possess a conserved isoprenylation motif and RabGGTase does not directly recognize its protein substrates. Instead, the Rab proteins are presented to the enzyme by means of an accessory factor, the Rab escort protein (REP). REP also delivers the Rab proteins to their target membranes after they have been isoprenylated by RabGGTase (Figure 1).^{4–6}

Rab proteins play key roles in the eukaryotic cell and it is therefore not surprising that an imbalance in Rab activity can lead to various types of disease. For example, overexpression of RabGGTase and its substrates such as Rab5a, Rab7, and Rab25 has been reported in several cancer types.^{7,8} Furthermore, elevated levels of Rab25 in breast and ovarian cancer cells were reported to increase aggressiveness of these cancers.^{9–11} These findings indicate that RabGGTase may be a promising target for cancer chemotherapy. Indeed, it has recently been shown that inhibition of RabGGTase induces p53-independent apoptosis,¹² and it was also proposed that the inhibition of RabGGTase is responsible for the proapoptotic action of several FTase inhibitors that are currently in late-stage clinical trials.¹³

This demonstrates that absolute target specificity may not be required and in fact cross-reactivity may be desirable to successfully treat isoprenyl transferase-linked disease, which is also in line with data obtained with numerous kinase inhibitors that have been developed by the pharmaceutical industry.¹⁴ On the other hand, a thorough investigation of

[†]PDB ID codes: crystal structures of engineered RabGGTase in complex with different inhibitors have been deposited with PDB ID codes 3HXB, 3HXC, 3HXD, 3HXE, and 3HXF.

*To whom correspondence should be addressed. Phone: +49 231 133 2364. Fax: +49 231 133 2399. E-mail: wulf.blankenfeldt@mpi-dortmund.mpg.de.

^a Abbreviations: FPP, farnesyl pyrophosphate; FTase, farnesyltransferase; GGPP, geranylgeranyl pyrophosphate; GGTase-I, geranylgeranyl transferase I; REP, Rab escort protein; RabGGTase, Rab geranylgeranyl transferase.

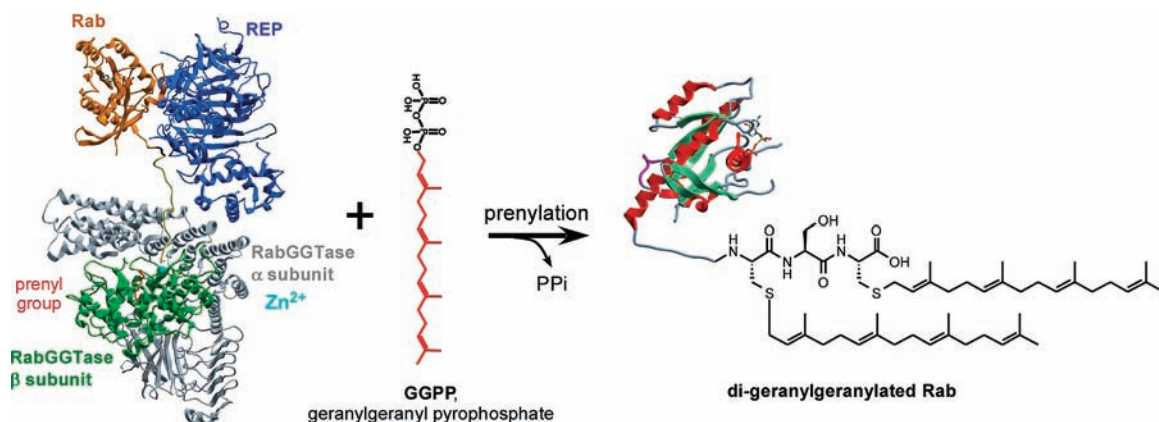


Figure 1. Geranylgeranylation of RabGTPases by RabGGTase.

RabGGTase and its protein substrates in biochemistry, cell biology, and disease would be greatly facilitated by the availability of highly specific RabGGTase inhibitors that also possess *in vivo* activity. However, compared to the situation for FTase^{15,16} and GGTase-I,^{17,18} the development of such inhibitors has lagged behind and only recently a handful of compounds have become available. Among these are two phosphonocarboxylate derivatives, which were found to inhibit only the second geranylgeranylation step of RabGTPases.¹⁹ As a consequence, these molecules are inactive against cellular processes mediated by Rab proteins that are only monogeranylgeranylated, such as Rab8, Rab13, Rab18, or Rab23. Moreover, the phosphonocarboxylates are not highly effective and need to be applied in high concentrations (0.1–1 mM) to inhibit RabGGTase *in vivo*.¹⁹ Nevertheless, they have been considered as lead structures in the development of new therapeutics for osteoporosis.^{20–22} Another promising compound class is formed by pyrrolidine-based inhibitors,^{23,24} which were developed from GGTase-I inhibitors.^{23,24} However, even though these compounds exhibit low micromolar IC₅₀ values against RabGGTase *in vitro*, they do not display high activity in cell-based assays.^{24,25}

One problem in the development of new RabGGTase inhibitors lies in the fact that the active sites of FTase, GGTase-I, and RabGGTase are conserved, thereby increasing the likelihood of cross-inhibition. A second challenge comes from the enlarged size of the RabGGTase active site, which has evolved to accommodate a large variety of different Rab protein C-termini^{5,26} and which makes it difficult to target with small molecules.

Bioactive natural products are a naturally evolved rich source of small molecules for chemical biology and medicinal chemistry research.^{27,28} In the case of isoprenoid transferases, the natural tripeptide pepticinnamin E from *Streptomyces* OH-4652, which is an inhibitor of FTase (Figure 2),^{29,30} may be a good starting point for the development of RabGGTase-specific inhibitors. Peptide libraries are accessible by solid phase synthesis, and we have recently reported first examples of RabGGTase inhibitors from a pepticinnamin E inspired compound collection together with the first crystal structure of RabGGTase in complex with one inhibitor (Figure 3a,b). While this inhibitor was not specific for RabGGTase, the structure revealed additional anchor points that could be exploited to design more potent and selective antagonists. In addition, other compounds in this library displayed a high degree of selectivity for RabGGTase, which shows that these molecules provide a promising starting point for the

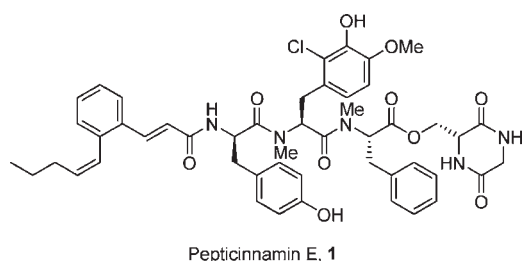


Figure 2. Structure of pepticinnamin E.

development of more potent and specific inhibitors.³¹ We have therefore explored this library to derive structure–activity relationships and to elucidate the binding modes displayed by the identified inhibitors in order to extract principles that may guide further design of peptidic and nonpeptidic inhibitors.

Results and Discussion

Solid Phase Synthesis of Inhibitors. To obtain a library of potential RabGGTase inhibitors a total of 66 peptides with a free C-terminus was synthesized on 2-chlorotrityl resin in 20–99% overall yield. Another group of 369 new peptides was produced by employing the hydrazide safety catch linker.^{32–36} For these molecules, one-step oxidative release with catalytic amounts of Cu(OAc)₂ gave higher yields after purification than the two-step NBS/pyridine protocol. In addition, fewer side products were formed. The difference was more pronounced when amine nucleophiles rather than alcohols were used. Furthermore, Cu(OAc)₂ also proved compatible with automated peptide synthesis. The yield ranged from 1–30% for inhibitors generated by this approach, and the purity of most peptides was higher than 95% after preparative HPLC. The library was further augmented by 34 pepticinnamin E derived FTase inhibitors,^{37–40} resulting in a total of 469 compounds further investigated here (Chart 1, Supporting Information Table S1).

Structure–Activity Relationship Analysis. The tripeptide library was screened for inhibitory activity toward RabGGTase using a solution-based continuous fluorometric assay adapted to a 384-well plate format.⁴¹ Out of 49 compounds that displayed inhibitory activity of more than 70% in the initial screen, 33 showed concentration-dependent inhibition and were selected for further studies. We observed a clear preference for tripeptides containing the aromatic amino acids histidine, phenylalanine, and tyrosine at all three

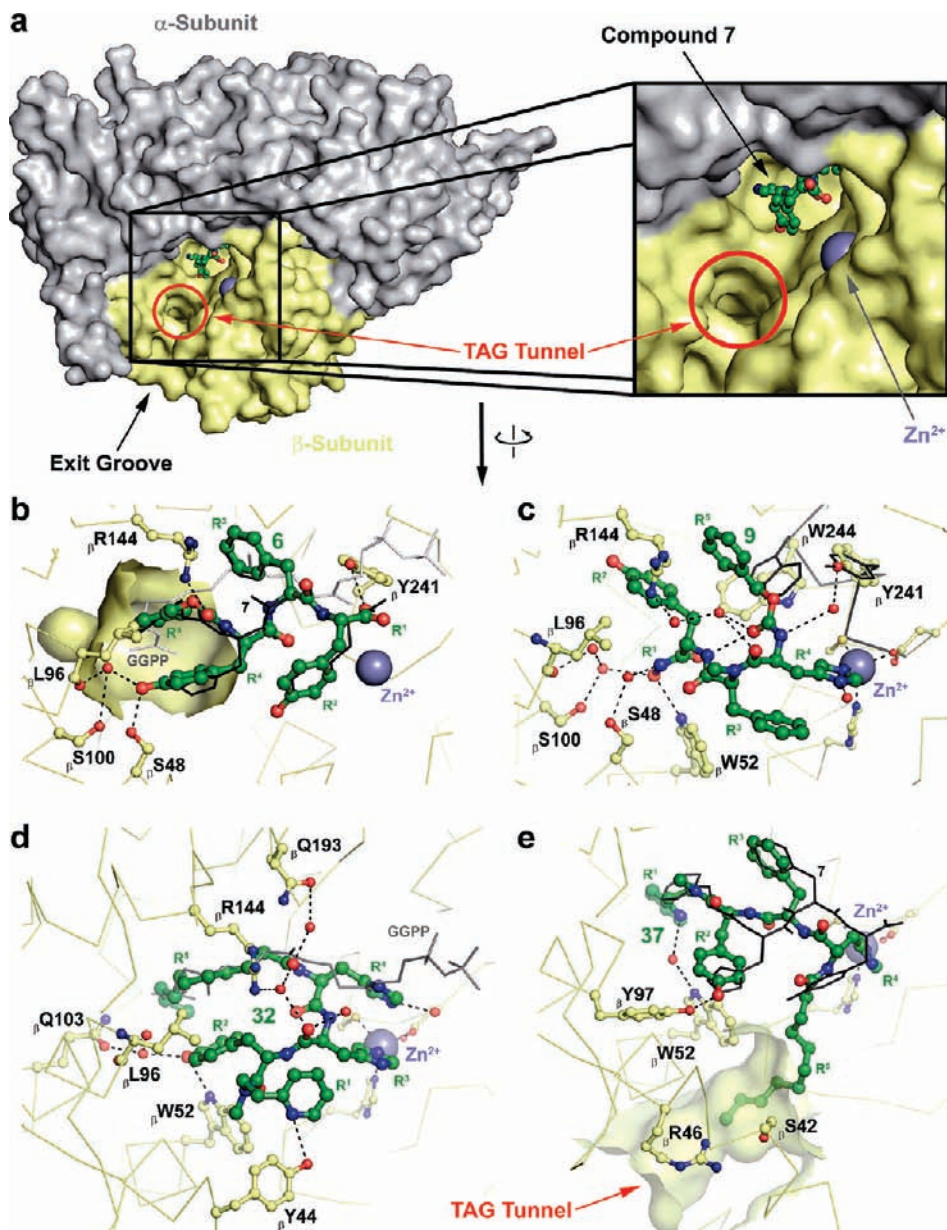


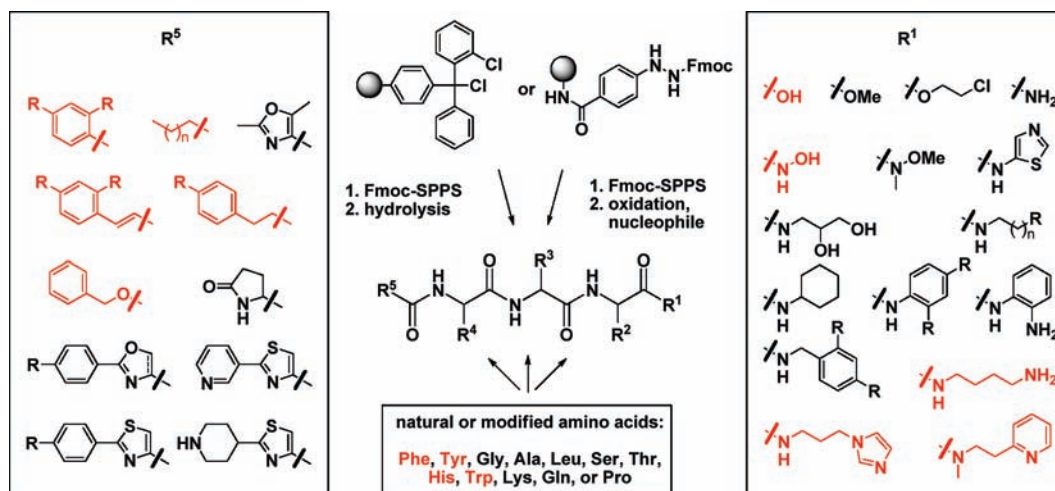
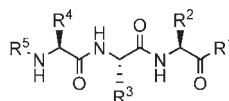
Figure 3. Binding of pepticinnamin E derived inhibitors to RabGGTase. (a) Surface representation of RabGGTase bound with class I inhibitor 7 (PDB entry 3C72). (b–e) Details of inhibitor binding. Residues from the α -subunit have been omitted for clarity, the view is rotated by 90° in the vertical paper plane with respect to (a). (b) Binding of inhibitor 6. The partial surface indicates the bottom of the GGPP binding site. Inhibitor 7 is shown in thin black, GGPP (PDB entry 3DST) in thin gray lines. (c) Binding of class I inhibitor 9. Thin black lines indicate the position of C240–V245 in the unliganded form. The orientation is similar to that of (b). (d) Binding of class III inhibitor 32. The lipid moiety at R^5 emulates the isoprenoid group of GGPP shown in thin gray lines. (e) Binding of compound 37. The lipid moiety binds to the TAG tunnel of RabGGTase (transparent surface). β S42 and β R46 provide additional polar anchor points for optimized derivatives of 37. Inhibitor 7 is shown in thin black lines for orientation.

positions (Tables 1–3). For example, the exchange of L-tyrosine for L-serine at position R^2 in compounds 32 and 36 led to an increase of the IC_{50} values from 11 and 5.2 μ M to over 100 μ M (Supporting Information Table S1, entry 84, compound 88; entry 367, compound 371).

For further analysis of structure–activity relationships, the most potent inhibitors retrieved from the compound library are grouped into three classes here depending on their N- and C-termini. The compounds possessing a free carboxylic or hydroxamic acid at their C-terminus ($R^1 = -OH$ or $-NH-OH$) and lipophilic N-termini ($R^5 =$ benzylloxycarbonyl, arylalkyl, cinnamyl, biaryl, etc.) are assigned to class I (Table 1). Class II inhibitors represent a

variation of class I, combining heterocyclic ring systems at their N-terminus with a free carboxylate at the C-terminus (Table 2). Finally, class III comprises compounds that contain lipophilic N-termini (long alkyl or *p*-alkoxybenzoyl groups) and an amine or N-heterocycle containing a C-terminal amide (Table 3).

Structure–Activity Relationship of Class I Inhibitors. To gain more insight into principles governing the binding of class I inhibitors, the most potent compound of this group 6 ($IC_{50} = 4.1 \pm 0.2 \mu$ M) was chosen for crystal structure analysis of the complex with RabGGTase. It was possible to derive the position and orientation of 6 unequivocally despite relatively poor electron density (Supporting

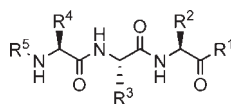
Chart 1. Representative Building Blocks Used in Fmoc-SPPS of the Tripeptide Library. Red Depicts Structural Features Found in the Best RabGGTase Inhibitors**Table 1.** Class I Inhibitors

Entry	Peptide	R ⁵	R ⁴	R ³	R ²	R ¹	IC ₅₀ (μM) ^a
1	6		D-Tyr	L-Phe	L-Tyr	OH	4.1 ± 0.2
2	7		L-His	L-(Me)Phe	L-Tyr	OH	22.7 ± 1.7
3	8		L-His	L-(Me)Phe	L-Trp	NH-OH	5.2 ± 0.6
4	9		L-His	L-(Me)Phe	L-Tyr	NH-OH	9.0 ± 1.0
5	10		L-His	L-(Me)Phe	D-Tyr	NH-OH	13.6 ± 1.1
6	11		D-Tyr	L-Tyr	L-Phe	OH	11.0 ± 1.4
8	12		D-His	L-(Me)Phe	L-Phe	OH	19.0 ± 3.8
9	13		D-His	L-Tyr	L-Phe	OH	15.6 ± 1.3
10	14		L-His	L-Tyr	L-Phe	OH	19.3 ± 3.6
11	15		D-His	L-Tyr	D-Phe	OH	15.2 ± 2.2
12	16		D-His	L-Tyr	L-Tyr	OH	22.7 ± 2.9

^aIC₅₀ values were calculated from three independent measurements.

Information Figure S1a), which is probably a consequence of incomplete occupancy due to low solubility of the inhibitor under the crystallization conditions. Compound **6**,

incorporating a D-amino acid at R⁴, binds very similarly to the previously investigated **7** by burying the benzoyl moiety at R⁵ in the isoprenoid pocket of the active site.³¹ The

Table 2. Class II Inhibitors

Entry	Peptide	R ⁵	R ⁴	R ³	R ²	R ¹	IC ₅₀ (μM) ^a
1	17		L-His	Gly	L-His(Trt)	OH	8.1 ± 1.0
2	18		L-His	Gly	L-His	OH	> 50
3	19		L-His(Trt)	Gly	L-His	OH	38 ± 8.7
4	20		His	Gly	L-Phe	OH	> 50
5	21		L-His(Trt)	Gly	L-Phe	OH	30 ± 1.8
6	22		Gly	L-Phe	L-His	OH	45 ± 21
7	23		Gly	L-Phe	L-His(Trt)	OH	25 ± 8.0
8	24		Gly	L-Phe	L-His(Bn)	OH	> 50
9	25		Gly	L-Phe	L-His(Boc)	OH	> 50
10	26		Gly	L-Phe	L-His	OH	> 50
11	27		Gly	L-Phe	L-His(Trt)	OH	46 ± 5.4
12	28		Gly	L-Phe	L-His	OH	41 ± 6.2
13	29		Gly	L-Phe	L-His(Trt)	OH	36 ± 5.7
14	30		Gly	L-Phe	L-His	OH	> 50
15	31		Gly	L-Phe	L-His(Trt)	OH	37 ± 2.0

^a IC₅₀ values were calculated from three independent measurements.

backbones of **6** and **7** adopt an extended, β -strand-like conformation such that the C-termini point outward, forming no contacts with the enzyme and remaining flexible, as indicated by high *B* factors. The only obvious difference between **6** and **7** is that a hydrogen bond between the histidyl side chain at R⁴ and β Y97 in **7** is replaced by a slightly more buried hydrogen bonding network involving the tyrosyl side chain at R⁴, β S48, and, through a water molecule, β L96 and β S100 (Figure 3b).

The structures of the complexes of RabGGTase with **6** and **7** showed that the N-terminal benzoyl group does not reach the bottom of the geranylgeranyl binding site and thus potentially misses an important anchor point (Figure 3b). This prompted us to synthesize class I inhibitors with longer N-termini (compounds **11**–**16**). However, this change did not yield better inhibitors.

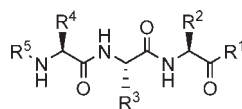
Because the C-termini of **6** and **7** point outward toward the catalytic Zn²⁺, we also synthesized analogues with a slightly longer C-terminus containing a hydroxamide moiety, which is a well-established zinc-binding group (compounds **8**–**10**, Table 1). This did indeed increase the potency (IC₅₀ = 9.0 ± 1.0 μM for **9** compared to IC₅₀ = 22.7 ± 2.9 μM for the corresponding inhibitor **7**). To corroborate that this improvement was due to Zn²⁺ coordination, the crystal structures of RabGGTase complexes with compounds **8** and **9** were determined (Figure 3c). Unexpectedly, this

revealed that these compounds bind in a different orientation. They are rotated by 180° with respect to **6** and **7**. As a consequence, the C-terminal hydroxamide group at R¹ does not bind to Zn²⁺ at the entrance to the active site but is located at the bottom of the GGPP binding pocket. The R¹ *N*-hydroxy group is anchored by a hydrogen bond to the side chain of β W52. In comparison, similar binding of the R¹ group of **6** and **7** to the geranylgeranyl binding site seems unfavored because the higher charge of their R¹ carboxylate groups does not match the properties of the binding site around β W52.

The backbones of inhibitors **8** and **9** adopt a turn-like conformation involving an intramolecular hydrogen bond between the carbonyl at R⁵ and the amide bond between R¹ and R². In contrast to inhibitors **6** and **7**, the peptide bond between R³ and R⁴ of **8** and **9** is in the *cis*-conformation, which is possible because *N*-methylation at R³ disrupts the rigidity of the peptide bond and decreases the energetic penalty for this otherwise unusual geometry.

Another important feature of inhibitors **8** and **9** is that their R⁴ histidyl residues coordinate to the Zn²⁺ cation of RabGGTase, indicating that it is indeed possible to target the reactive center of the active site. However, the binding energy gained by this interaction is apparently not high enough to orient inhibitor **7**, which differs only by having a free carboxylate at R¹, in a similar fashion to that of **9**.

Table 3. Class III Inhibitors



Entry	Peptide	R ⁵	R ⁴	R ³	R ²	R ¹	IC ₅₀ (μM) ^a
1	32		L-His	L-His	L-Tyr		11.0 ± 1.2
2	33		L-Tyr	L-His	L-Tyr	OMe	3.9 ± 0.2
3	34		L-Tyr	L-His	L-Tyr		6.3 ± 0.6
4	35		L-Tyr	L-His	L-Tyr		7.1 ± 0.3
5	36		L-His	L-His	L-Tyr		5.2 ± 0.7
6	37		L-His	L-Phe	L-Tyr		4.7 ± 0.1
7	38		L-His	L-Phe	L-Tyr		> 100
8	39		L-His	L-Phe	L-Tyr		2.8 ± 0.4
9	40		L-His	L-Phe	L-Tyr		26 ± 0.3
10	41		L-His	L-Phe	L-Tyr		> 100
11	42		L-Tyr	L-Tyr	L-Tyr		11.6 ± 1.2
12	43		L-His	L-His	L-His		12.1 ± 0.8
13	44		L-His	L-His	L-His		24.0 ± 1.4
14	45		L-His	L-Tyr	L-Phe		12.3 ± 0.6

^aIC₅₀ values were calculated from three independent measurements.

Unlike compounds **6** and **7**, binding of **8** and **9** leads to local changes in the protein structure with respect to the unliganded enzyme. Most notably, the first five residues of α -helix β D238– β G253 of the β -subunit adopt a 3_{10} -helical conformation in the complex, leading to a maximum C α displacement of 1.7 Å at β S242 (Figure 3c). This rearrangement is probably the consequence of a steric clash between R⁵ and the side chain of β W244, which rotates by 180° in χ_2 , thereby pushing aside residues β V239– β W243 and also the side chain of β Y195. Interestingly, a similar rearrangement is also observed upon binding of GGPP (PDB entry 3DST).⁵ Therefore, we propose that it presents a “cocking” mechanism in which the active site is primed for the catalytic cycle.

Structure–Activity Relationships of Class II Inhibitors. The binding pocket surrounding the N-terminal groups of **6** and **7** is relatively spacious, harbors several water molecules,

and also provides scattered polar attachment points. To explore whether the inhibition properties can be improved by better filling of this cavity and by introducing additional hydrogen bonds, class II inhibitors containing heterocycles at their N-termini and free carboxylates at the C-terminus were synthesized. In general, the resulting molecules showed only weak inhibition of RabGGTase (Table 2), but interestingly, compounds still carrying trityl (Trt) protecting groups showed higher activity than the corresponding unprotected molecules. For example, the most potent representative of this series is compound **17** (IC₅₀ = 8.1 ± 1 μM), an inhibitor containing a trityl-protected histidine. Removal of this group decreased the potency dramatically (compound **18**, IC₅₀ > 50 μM). Unfortunately, crystallization experiments with **17** were not successful, but because **17** contains a free C-terminus at R¹ and the trityl-protected

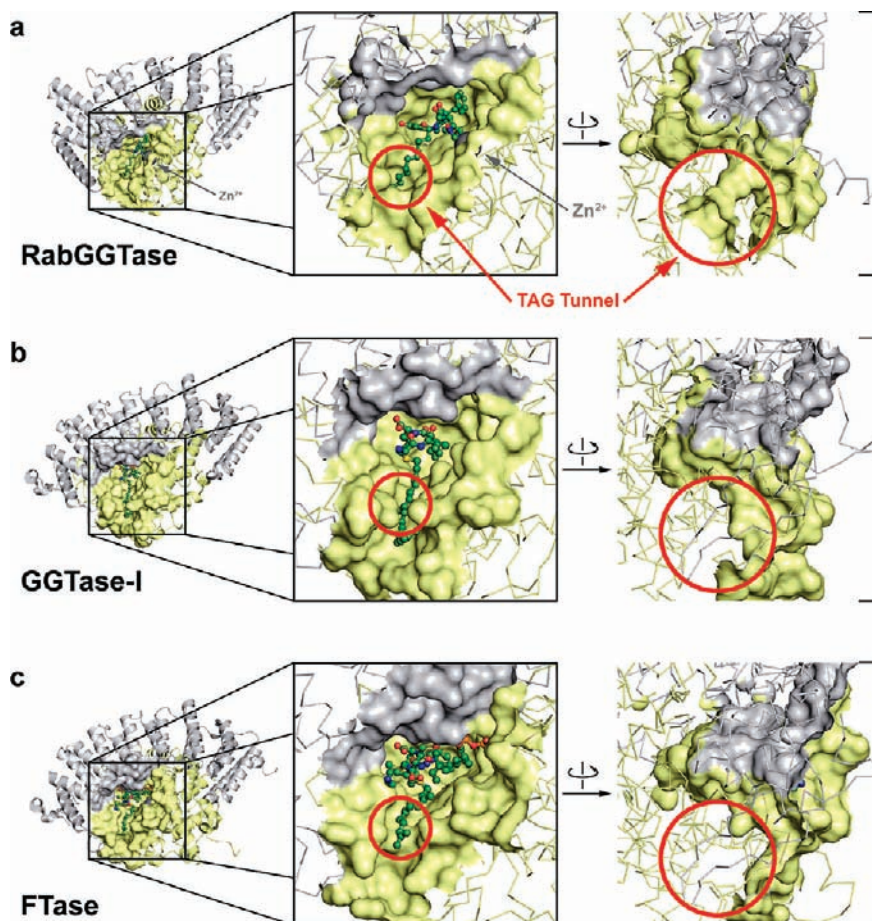


Figure 4. Active sites and exit grooves of RabGGTase (a), GGase-I (b, PDB entry 1N4S⁴³) and FTase (c, PDB entry 1KZO⁴²). RabGGTase is shown in complex with inhibitor **37**. Red circles mark the position of the TAG tunnel of RabGGTase.

histidine at R² is too large to be accommodated within the isoprenoid binding pocket, it is conceivable that **17** binds in a fashion similar to **6** and **7** with the C-terminus pointing outward. The modified side chain of R² is then expected to adopt a “gatekeeper” function, controlling access to the GGPP binding site as has been postulated for R² in **7**.³¹ This is further corroborated by fluorescence titration, which shows that **17**, like **7**, is competitive with respect to isoprenoid pyrophosphate (see below, Figure 5f, Supporting Information Figure S2).

Structure–Activity Relationships of Class III Inhibitors.

Because the crystal structures of RabGGTase complexed with **6** and **7** suggested that the inhibitors’ N-termini occupy the lipid binding region of the GGPP binding site, class III inhibitors containing an alkylaryl or a *p*-undecanoylbenzoyl moiety (lipid chain) at R⁵ were generated to enhance the association with the lipid binding site. Nitrogen-containing heterocycles or amines were introduced at R¹ to increase the chance of coordinating the Zn²⁺ cation. As can be seen in Table 3, this strategy produced a number of potent inhibitors with IC₅₀ values in the low micromolar range.

Two class III inhibitors, compounds **32** and **37**, were selected for crystal complex structure analysis because they displayed different inhibition modes with respect to the isoprenoid substrate (described below). Similar to class I inhibitors **6** and **7**, the N-terminus of compound **32** is buried in the lipid binding pocket of the GGPP site, but in comparison to these compounds, the lipid group of **32** extends deeper into the cavity, taking the position of the geranylgeranyl

chain of GGPP (Figure 3d). The inhibitor also binds the zinc ion of the active center, but it utilizes its R³ histidine side chain for coordination, not the one at R⁴ like the inhibitors **8** and **9**. Further, compound **32** displays a bent conformation such that the tyrosyl side chain of R² points back into the lipid binding pocket where it forms hydrogen bonds with βW52 similar to the hydroxamide moieties of **8** and **9**. In addition, R² engages in two water-mediated hydrogen bonds to βS100 and βQ103. The interaction of tyrosine at R² appears important for the binding of the compound because changing this residue to serine or histidine significantly reduces the inhibitory activity (Supporting Information Table S1, entry 84, compound **88**; entry 94, compound **98**). The bent conformation is also stabilized by a water molecule bound to βR144 and chelated between the carbonyl groups of R³ and R⁵, and by another water molecule that sits between the carbonyl of R⁵ and the side chain of βQ193. Sterically, the bent structure of **32** seems only possible because the lipid moiety at R⁵ does not completely fill the GGPP binding pocket and leaves free space for the side chain of R². One more direct hydrogen bond between βY44 and the pyridyl moiety at R¹ of inhibitor **32** seems to be formed, however the relatively low electron density indicates that this R¹ group is flexible (Figure 3c). Further, the amide bond between R¹ and R² is in the cis-conformation, which is probably a consequence of *N*-methylation at R¹. In addition, binding of **32** leads to similar structural changes of βV239–βW243 as have been observed in binding of inhibitors **8** and **9** or GGPP.

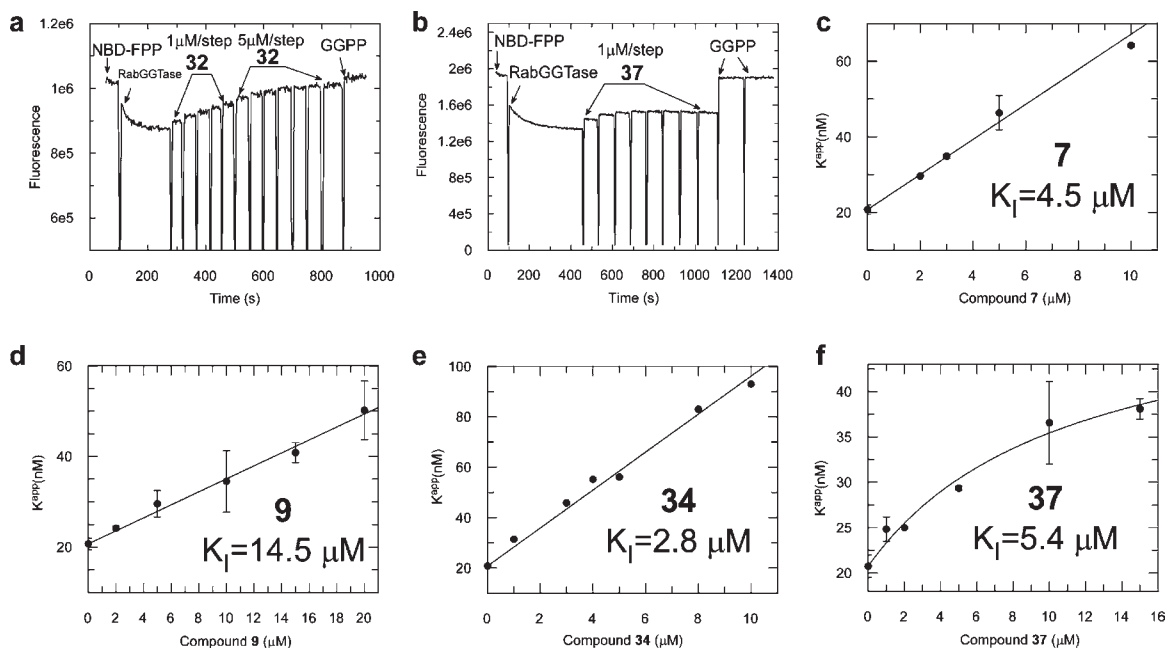


Figure 5. Analysis of the interaction of inhibitors with RabGGTase. (a) A displacement titration of **32** into NBD-FPP:RabGGTase complex followed by the addition of GGPP. (b) A similar experiment with compound **37**. The initial level of fluorescence represents the fluorescence of free NBD-FPP (400 nM). In the first titration step, RabGGTase was added to reach a concentration of 550 nM. Subsequently, compound **37** was titrated into the cuvette in 1 μ M steps. Finally, GGPP was added to a final concentration of 4 μ M. (c–f) The apparent K_d values of Mant-FPP interaction with RabGGTase in the presence of different concentrations of inhibitor **7** (c), **9** (d), **34** (e), and **37** (f). The data were fitted with a competitive (c–e) or partially competitive function (f) to obtain a dissociation constant (K_I) of the inhibitor with RabGGTase.

Similar to the case of class I inhibitors, changing only one amino acid at R^3 in inhibitor **32** to compound **37** leads to binding in a completely different manner (Figure 3e). Inhibitor **37** also induces local reorganization in β V239– β W243 as described above, but it is the C-terminal *N*-methyl-ethylpyridyl moiety at R^1 that associates with the lipid binding region of the GGPP pocket, i.e., the orientation of this inhibitor is inverted with respect to **32**, a similar change in orientation as has been observed with the two groups of class I inhibitors described above. R^1 of **37** extends as deeply in the isoprenoid binding pocket as the undecanoyl chain at R^5 of **32**. It is held in place by a water-mediated hydrogen bond to the side chain of β W52 and by π -stacking with the side chain of β W244. These interactions seem important because changing only R^1 decreased the potency of derivatives of **37** dramatically (Supporting Information Table S1, entries 42–53, compounds **46**–**57**). Notably, omitting only the methyl group of *N*-methyl-ethylpyridyl at R^1 in compound **38** abolished the inhibitory activity nearly completely. This probably reflects the fact that in **37**, similar to **32**, the amide bond between R^1 and R^2 adopts the *cis*-conformation, which leads to the correct positioning of the pyridyl moiety. Deletion of the methyl group apparently renders the *cis*-conformation energetically too disfavored and hence prevents binding of the pyridyl ring of **38** in the isoprenoid binding pocket.

The backbone of **37** is more extended than that of **32** such that it closely follows those of the class I inhibitors **6** and **7**, albeit with inverted direction (Figure 3e). As a consequence, the tyrosyl side chain at R^2 forms a tight hydrogen bond ($d = 2.8$ Å) to the side chain of β Y97, and the phenyl ring of R^3 occupies the same position as that of **6** and **7**. Other than in these structures, however, the histidine residue at R^4 is not disordered but tightly interacts with the Zn^{2+} of the active center. This tight interaction appears to be important and

may be the reason for the different orientations of **32** and **37**, where Zn^{2+} -binding was provided by R^3 instead.

Another striking feature of this complex is the observation that the lipid chain of **37** locates to a tunnel adjacent to the GGPP binding site, which we will refer to as the “TAG tunnel”. This tunnel, which is located in a region termed “exit groove” in the related CAAX box isoprenoid transferase,^{42,43} is not present in FTase or GGTase-I (Figure 4). It opens to the distal surface of RabGGTase and is lined by β -subunit residues with mixed chemical character (β I27, β Y30, β G31, β Y39, β S42, β R46, β L45, β V50, β W52, β L54, β P288), suggesting that optimal targeting of this site will require fine-tuning of the respective inhibitor moiety. This may also be reflected by the observation that the lipid moiety of **37** shows considerably higher average *B* factors (70 Å²) than the rest of the molecule (40 Å²; Supporting Information Figure S1d) and that binding of **37** and related compounds was sensitive to the length of the lipid chain, whereas shortening by three methylene units increased the potency to $IC_{50} = 2.8 \pm 0.4$ μ M (Table 3, entry 8, compound **39**), while shortening by another four units abolished binding completely (Table 3, entry 10, compound **41**). Extending the C-10 chain of **37** to a C-14 chain also led to a marked decrease in potency (Table 3, entry 9, compound **40**). This suggests that the TAG tunnel can only accommodate a lipid chain with an appropriate length: chains that are too short may not provide enough binding energy, whereas those that are too long may not match the electrostatic properties of the TAG tunnel. Because the TAG tunnel is an additional feature of the exit groove that is not present in FTase and GGTase-I, it is a promising anchor point for the development of specific inhibitors.

Analysis of Binding Modes and Affinities of Inhibitors. The determined IC_{50} values provide a measure of the inhibitory activity but do not give direct information on either their mode of action or their affinity for RabGGTase. In addition,

Table 4. Dissociation Constants (K_i) of Inhibitors for RabGGTase

entry	peptide	K_i (μ M)
1	7	4.5
2	9	14.5
3	17	5.3
4	32	1.1
5	34	2.8
6	37	5.4

correlating the complex structures with a quantitative analysis of the interaction between inhibitors and RabGGTase will provide more detailed insight into the mechanism of inhibition. To this end, we took advantage of the fluorescence change upon binding of the GGPP analogue NBD-FPP ({3,7,11-trimethyl-12-(7-nitrobenzo[1,2,5]oxadiazol-4-ylamino)-dodeca-2,6,19-trien-1} pyrophosphate) or Mant-FPP (*N*-methylantranilate farnesyl pyrophosphate) to RabGGTase.^{44,45} Using this signal, K_d values of 160 ± 3 nM and 21 ± 1 nM were obtained for the NBD-FPP and Mant-FPP interactions with RabGGTase, respectively (data not shown). To resolve the binding modes and affinities of our inhibitors with RabGGTase, two titration strategies were used. One was displacement titration, where the inhibitor is titrated into the preformed NBD-FPP:RabGGTase complex. The other was co-titration, where Mant-FPP is titrated with RabGGTase in the presence of various concentrations of inhibitor to obtain apparent K_d values.

Class I compounds **6** and **7**, class II compound **17**, and class III compounds **32**, **34**, and **37** were subjected to fluorescence titration. The fluorescence intensity of NBD-FPP decreased after addition of RabGGTase, indicating binding of NBD-FPP to the enzyme (Figure 5a,b). As shown in Figure 5b, titration of compound **32** into RabGGTase:NBD-FPP resulted in a dose-dependent increase in fluorescence intensity that saturated with complete recovery of unbound NBD-FPP fluorescence. Compounds **7**, **9**, **17**, and **34** display similar effects in the displacement titration (not shown), suggesting that these inhibitors compete with NBD-FPP. In contrast, titration of class III inhibitor **37** led to only partial recovery of NBD fluorescence (Figure 5b). This would mean that **37** either induced only partial displacement of NBD-FPP or that binding of **37** induces a fluorescence change of the bound NBD-FPP through an allosteric mechanism.

To distinguish between these two scenarios for the binding of **37** and to confirm the binding modes of other compounds, a set of co-titration experiments was performed. As shown in Figure 5c–f, the presence of inhibitors reduced the affinity of Mant-FPP for RabGGTase in a dose-dependent manner. According to a theoretical model of competitive or partially competitive inhibition, the apparent K_d values should display linear or hyperbolic relationships with the concentration of inhibitor, respectively. Therefore, compound **7**, **9**, and **34** are competitive with respect to isoprenoid pyrophosphate, whereas compound **37** is partially competitive (Figure 5c–f). Fitting the data to the corresponding functions yields the dissociation constants (K_i) shown in Table 4. Compounds **17** and **32** had already been confirmed previously as competitive inhibitors by co-titration experiments using NBD-FPP.³¹

The binding modes derived from this quantitative analysis correlate well with the crystal structure analysis. Compounds **7** and **9** associate with the isoprenoid binding pocket and are hence competitive with respect to the isoprenoid pyrophosphate

Table 5. IC₅₀ Values of Inhibitors for FTase, GGTase-I, and RabGGTase Determined by SDS-PAGE End Point Assay

entry	peptide	RabGGTase	FTase	GGTase-I
1	17	14 ± 1.3	13 ± 1.0	6.9 ± 2.3
2	19	41 ± 4.0	14 ± 2.6	2.6 ± 1.0
3	23	31 ± 8.3	3.4 ± 0.7	5.6 ± 2.0
4	32	10 ± 0.9	35 ± 5.8	60 ± 5.3
5	34	4.3 ± 0.4	> 100	> 100
6	37	2.8 ± 0.1	> 100	> 100
7	39	8.8 ± 0.7	98 ± 4.7	97 ± 3.1

even though these two molecules bind RabGGTase in different orientations. The co-crystal structure of RabGGTase:**17** is not available, but from the titration data it can be concluded that **17** binds in a manner similar to **7**.

Interestingly, compounds **32** and **37**, which differ only at position R³, nevertheless display significantly different inhibition modes. While **32** is competitive with respect to the GGPP analogue NBD-FPP, inhibitor **37** is only partially competitive, which indicates that it binds to a site different from the isoprenoid binding pocket and that this interaction cannot be completely abrogated even by very high concentrations of isoprenoid substrate.

Selectivity toward RabGGTase, GGTase-I, and FTase. The selectivity of representative RabGGTase inhibitors toward all protein isoprenyl transferases was assessed using an SDS end-point assay.³¹

As can be seen in Table 5, several compounds showed marked preference for RabGGTase, with selectivity reaching nearly 50-fold in the best cases. Most prominent examples belong to class III compounds, with inhibitor **37** having the highest selectivity of all inhibitors tested. Because **37**, unlike most other inhibitors, is only partially competitive with respect to the GGPP analogue NBD-FPP, it is interesting to note that the other known RabGGTase-selective, pyrrolidine-based, and phosphonocarboxylate inhibitors were also found not to compete with GGPP but with RabGGTase binding instead.^{19,24} Therefore, one could speculate that these compounds also target the TAG tunnel. If this hypothesis is correct, it would lead to the assumption that the TAG tunnel plays a role in positioning the monogeranylgeranylated RabGGTase for the second isoprenoid transfer because the phosphonocarboxylate inhibitors inhibit only this second geranylgeranylation.¹⁹ This was, however, not observed in our previous study employing geranylgeranylated peptides,⁵ indicating that further experiments are required to clarify this interesting mechanistic question.

In the case of compound **32**, which is a competitive inhibitor with respect to the isoprenoid pyrophosphate, selectivity was increased considerably by a single replacement of histidine with tyrosine at R⁴ in compound **34**. This shows that selective inhibitors can also be obtained without losing the ability to exclude GGPP from the active site.

In Vivo Activity of RabGGTase Inhibitors. To assess the suitability of the developed compounds for in vivo analysis, we assessed their activity and toxicity on cultured COS-7 cells. No cytotoxicity was observed when COS-7 cells were incubated with 100 μ M of inhibitors **8**, **9**, **17**, **32**, **34**, or **37**. The in vivo activity was assessed by quantifying the prenylation of overexpressed EYFP-Rab7 fusion protein. The prenylation status of the protein was assessed by its ability to be prenylated in cellular lysates using a biotinylated analogue of GGPP, followed by subsequent detection with streptavidin-coupled horseradish peroxidase in a Western blot

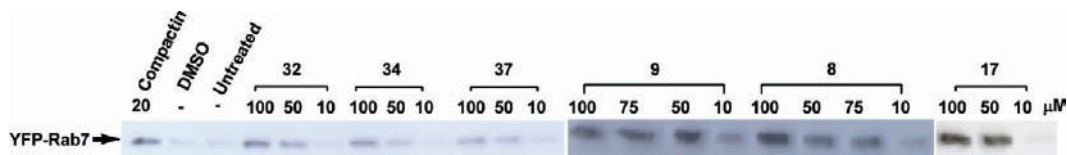


Figure 6. Western Blot of *in vivo* activity assay in COS-7. Cells overexpressing YFP-Rab7 were treated with 20 μ M compactin, which inhibits the synthesis of isoprenyl lipid, as a positive control and with 1/1000 v/v DMSO as a negative control. The inhibitors were screened at three different concentrations, 100, 50, and 10 μ M. Cell lysates were prenylated *in vitro* with biotin labeled geranylgeranyl analogues, resolved by SDS-PAGE, Western blotted, and analyzed with streptavidin–HRP. The bands corresponding to YFP-Rab7 were quantified.

Scheme 1. Fmoc Solid Phase Peptide Synthesis Using the Hydrazide Linker

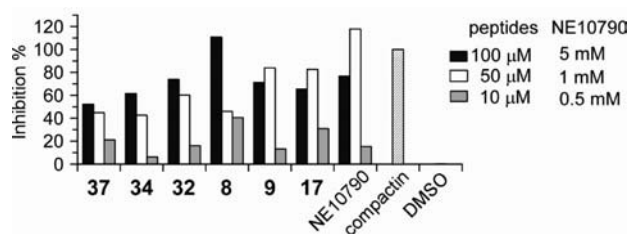
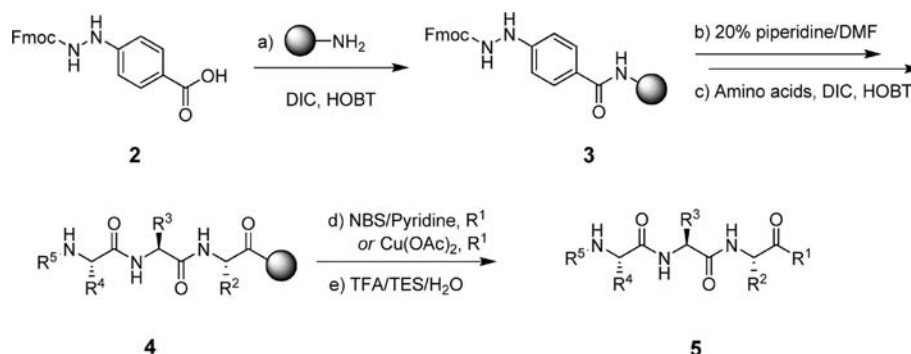


Figure 7. Relative amount of inhibition of by six peptide inhibitors. The relative amount of inhibition at different concentrations was calculated by integration of the intensity of the corresponding EYFP-Rab7 blot bands (Figure 6). The band intensity of the inhibitors was normalized against the band intensity induced by compactin and DMSO.

(Figure 6).^{25,31} All compounds inhibited geranylgeranylation in a dose-dependent manner, indicating their general cell permeability. Nearly the same level of inhibition as obtained with the mevalonate pathway inhibitor compactin was achieved with the nonspecific class I and II inhibitors **8**, **9**, and **17**, whereas class III inhibitors **32**, **34**, and **37** inhibited RabGGTase to approximately 70% of the compactin level within the concentration range tested (Figure 7). These experiments show that the peptidic inhibitors here are indeed promising candidates for the analysis of Rab prenylation *in vivo* and its importance in cell physiology and disease processes.

Conclusions

Several obstacles make the development of selective and potent inhibitors of RabGGTase challenging. First, related prenyltransferases that catalyze similar reactions in other pathways exist in the eukaryotic cell, increasing the possibility of off-target effects. Second, the active site of RabGGTase is relatively unspecific toward both the isoprenoid and the protein substrate,^{5,26} and *in vivo* the protein substrate specificity is conferred by the accessory protein REP. Third, related to this problem is the fact that the active site of RabGGTase is

large and not easy to target by small-molecule compounds with drug-like properties. All this also makes it difficult to derive firm structure–activity relationships that could guide inhibitor design.

Using the tripeptidic FTase inhibitor peptidicinnamin E as a starting point, we have synthesized a peptide library augmented by incorporation of unnatural N- and C-termini to target specific features in the active site of RabGGTase. Screening of the library revealed several potent binders displaying different inhibition modes. This was also corroborated by crystal structure analysis, showing that inhibiting compounds can adopt different conformations and orientations in the active site. They can also target various areas of the active site, including polar and hydrophobic regions of the isoprenoid binding pocket, the catalytic Zn²⁺ cation, and the TAG tunnel located inside the exit groove. The changes in binding mode were triggered by only small variations in the inhibitor's structure. This indicates that several factors contribute to the positioning of the inhibitor and that none of these factors is dominant, i.e., the binding energy landscape is relatively flat. It should therefore be possible to improve the binding affinity by synthesizing inhibitors that combine the various interaction motifs observed in this study.

Several potent inhibitors with high selectivity for RabGGTase were retrieved from the library. The most selective compounds were found to bind in a partially competitive inhibition mode with respect to the isoprenoid pyrophosphate. The crystal structure revealed that these compounds, in contrast to the less selective molecules investigated, bind to the TAG tunnel. Because this region of RabGGTase is considerably different from the corresponding regions in FTase and GGTase-I, it provides the most attractive avenue for further selectivity improvement.

Finally, the developed peptidic inhibitors were not toxic and displayed activity in cell-based assays. Together, these data show that it is indeed possible to synthesize potent and selective peptide-based inhibitors for RabGGTase. In future

work, we will employ the extensive structural, biophysical, and cellular activity data obtained in this study to develop potent and specific RabGGTases inhibitors as potential guiding structures for novel pharmaceuticals.

Experimental Section

For full details, refer to the online Supporting Information.

Synthesis of Peptide Inhibitors. The 469 inhibitors investigated here were synthesized as described previously.^{32–36} Briefly, an Fmoc-based solid phase synthesis strategy was employed. Structural variation included different aliphatic (e.g., Ala, Gly, Leu, Pro), aromatic (His, Phe, Trp, Tyr), and polar (Ser, His, Lys, Gln, Glu, Thr) D- and L-amino acids, various long and short chain aliphatic, olefinic, aromatic, biphenyl, and heteroaromatic amides at the N-terminus and saturated and unsaturated esters as well as aliphatic and aromatic amides at the C-terminus. Peptides with a free carboxylic acid at the C-terminus were generated by coupling to 2-chlorotrityl resin followed by acidic release from the solid phase. Other C-termini were generated by using the hydrazide safety catch linker.^{32–36} In these cases, release from the resin was achieved by oxidation of the linker with stoichiometric amounts of NBS/pyridine or with catalytic quantities of Cu(OAc)₂, followed by nucleophilic attack with various reagents (Scheme 1). Protecting groups were subsequently removed with TFA/ TES/H₂O (50:1:1), and the resulting products were purified by HPLC. Purity was controlled by HPLC and NMR and was usually higher than 95%. The structure and diversity of the used amino acids and building blocks of the collection are illustrated in Chart 1.

Cloning, Protein Expression and Purification. Rat FTase, GGTase-I, RabGGTase, REP-1, human GST-KiRas, human GST-RhoA, and canine Rab7 were produced as recombinant proteins as described earlier.⁴⁴ For crystallization, we used an engineered version of RabGGTase in which two domains not participating in catalysis have been deleted.^{5,31}

Quantitative Analysis of RabGGTase Inhibition. The inhibitor library was screened in a continuous assay based on the large fluorescence increase of an analogue of GGPP ({3,7,11-trimethyl-12-(7-nitrobenzo[1,2,5]oxadiazol-4-ylamino)-dodeca-2,6,19-trien-1} pyrophosphate, NBD-FPP), observed after its conjugation to Rab7 by RabGGTase in the presence of REPI. In the typical assay Rab7 (3 μ M) and REPI (3 μ M) were combined with NBD-FPP (9 μ M) and 400 nM RabGGTase in the presence or absence of inhibitor.^{41,46,47} The assay was adapted to 96- and 384-well plate format and inhibitors, leading to a decrease of RabGGTase activity of more than 70% at 100 μ M were selected for concentration-dependent inhibition studies, yielding the IC₅₀ values summarized in Supporting Information Table S1.⁴¹

To gain more detailed insight into the mode of action of selected inhibitors, fluorescence titrations monitoring the signal of NBD-FPP on displacement of RabGGTase were performed. In this case, 400 nM of NBD-FPP were first equilibrated with 550 nM RabGGTase and inhibitors were added in 1 or 5 μ M steps. End points were controlled by final addition of 4 μ M GGPP. For further confirmation of the binding mode derived from this experiment, RabGGTase in the presence of different inhibitor concentrations was titrated to a solution of 300 nM Mant-FPP to obtain a series of apparent K_d^{app} values for Mant-FPP by fitting to a quadratic equation as described elsewhere.⁴⁶

Crystal Structure Analysis of RabGGTase:Inhibitor Complexes. Crystallization experiments were performed with an engineered form of RabGGTase lacking the LRR- and Ig-domains.⁵ Complexes were either prepared by soaking or by co-crystallization.³¹ Diffraction data were collected at 100 K on station X10SA of the Swiss Light Source (Villigen, Switzerland).

Data reduction in XDS⁴⁸ and refinement with REFMAC5,⁴⁹ COOT,⁵⁰ and PRODRG⁵¹ was performed following standard procedures, applying partial occupancies to ligands to match the *B* factors of neighboring protein residues in some cases. Data collection and refinement statistics are shown in Supporting Information Table S2, $|F_O - F_C|$ difference electron densities are shown in Supporting Information Figure S1.

Assessment of Selectivity toward RabGGTase, GGTase-I, and FTase. The selectivity of several inhibitors toward the three eukaryotic prenyltransferases was judged by an SDS-PAGE end point assay, using NBD-GPP or NBD-FPP, respectively. The enzymes were allowed to transfer these fluorescent prenyl substrate analogues to their substrate proteins (GST-KiRas, GST-RhoA, or Rab7) in the presence of different concentrations of inhibitor for 10 min, reactions were quenched by SDS-sample buffer and were subjected to SDS-PAGE. Fluorescent bands were quantified by densitometry and the data were processed as described elsewhere.³¹

Inhibition of RabGGTase Activity in Cultured Cells. In vivo activity was analyzed by exposing COS-7 cells transiently transfected with EYFP-Rab7 fusion protein to various concentrations of putative RabGGTase inhibitors. Cells were lysed after 24 h, and the clarified supernatant was incubated with biotinylated geranyl pyrophosphate (biotin-GPP), recombinant RabGGTase, and REP, followed by separation with SDS-PAGE. Unprenylated YFP-Rab7 in cells was biotin-geranylated and was subsequently resolved by Western blot and with streptavidin–HRP.²⁵

Acknowledgment. This work was partially supported by scholarships of the International Max Planck Research School in Chemical Biology (to K.T.T.), the Alexander von Humboldt Foundation (to R.S.B.), and by a Heisenberg award from the Deutsche Forschungsgemeinschaft (to K.A.). Funding was provided by the Centre for Applied Chemical Genomics and by DFG grants AL 484/7-2 (to K.A.) and SFB642 (to K.A., R.S.G., and H.W.). We thank the X-ray communities of the Max-Planck-Institute of Molecular Physiology (Dortmund, Germany) and of the Max-Planck-Institute for Medical Research (Heidelberg, Germany) for collecting diffraction data. The beamline staff at station X10SA of the Swiss Light Source of the Paul Scherrer Institute (Villigen, Switzerland) is gratefully acknowledged for giving us generous access to their facilities.

Supporting Information Available: Complete list of inhibitors and their inhibitory potency, X-ray data collection, and refinement statistics, $|F_O - F_C|$ difference electron density maps, analysis of the interaction of **17** with RabGGTase determined by fluorescence titration, full experimental details, analytics of compounds synthesized. This material is available free of charge via the Internet at <http://pubs.acs.org>.

References

- (1) Leung, K. F.; Baron, R.; Seabra, M. C. Thematic review series: lipid posttranslational modifications. geranylgeranylation of Rab GTPases. *J. Lipid Res.* **2006**, *47*, 467–475.
- (2) Zerial, M.; McBride, H. Rab proteins as membrane organizers. *Nat. Rev. Mol. Cell Biol.* **2001**, *2*, 107–117.
- (3) Miaczynska, M.; Christoforidis, S.; Giner, A.; Shevchenko, A.; Uttenweiler-Joseph, S.; Habermann, B.; Wilm, M.; Parton, R. G.; Zerial, M. APPL proteins link Rab5 to nuclear signal transduction via an endosomal compartment. *Cell* **2004**, *116*, 445–456.
- (4) Alexandrov, K.; Horiuchi, H.; Steele-Mortimer, O.; Seabra, M. C.; Zerial, M. Rab escort protein-1 is a multifunctional protein that accompanies newly prenylated rab proteins to their target membranes. *EMBO J.* **1994**, *13*, 5262–5273.
- (5) Guo, Z.; Wu, Y. W.; Das, D.; Delon, C.; Cramer, J.; Yu, S.; Thuns, S.; Lupilova, N.; Waldmann, H.; Brunsfeld, L.; Goody, R. S.;

- Alexandrov, K.; Blankenfeldt, W. Structures of RabGGTase-substrate/product complexes provide insights into the evolution of protein prenylation. *EMBO J.* **2008**, *27*, 2444–2456.
- (6) Pylpyenko, O.; Rak, A.; Reents, R.; Niculae, A.; Sidorovitch, V.; Cioaca, M. D.; Bessolitsyna, E.; Thoma, N. H.; Waldmann, H.; Schlichting, I.; Goody, R. S.; Alexandrov, K. Structure of Rab escort protein-1 in complex with Rab geranylgeranyltransferase. *Mol. Cell* **2003**, *11*, 483–494.
- (7) Croizet-Berger, K.; Daumerie, C.; Couvreur, M.; Courtoy, P. J.; van den Hove, M. F. The endocytic catalysts, Rab5a and Rab7, are tandem regulators of thyroid hormone production. *Proc. Natl. Acad. Sci. U.S.A.* **2002**, *99*, 8277–8282.
- (8) He, H.; Dai, F.; Yu, L.; She, X.; Zhao, Y.; Jiang, J.; Chen, X.; Zhao, S. Identification and characterization of nine novel human small GTPases showing variable expressions in liver cancer tissues. *Gene Expression* **2002**, *10*, 231–242.
- (9) Cheng, K. W.; Lahad, J. P.; Kuo, W. L.; Lapuk, A.; Yamada, K.; Auersperg, N.; Liu, J.; Smith-McCune, K.; Lu, K. H.; Fishman, D.; Gray, J. W.; Mills, G. B. The RAB25 small GTPase determines aggressiveness of ovarian and breast cancers. *Nat. Med.* **2004**, *10*, 1251–1256.
- (10) Cheng, K. W.; Lahad, J. P.; Gray, J. W.; Mills, G. B. Emerging role of RAB GTPases in cancer and human disease. *Cancer Res.* **2005**, *65*, 2516–2519.
- (11) Gonzalez-Santiago, L.; Alfonso, P.; Suarez, Y.; Nunez, A.; Garcia-Fernandez, L. F.; Alvarez, E.; Munoz, A.; Casal, J. I. Proteomic analysis of the resistance to apilidin in human cancer cells. *J. Proteome Res.* **2007**, *6*, 1286–1294.
- (12) Lackner, M. R.; Kindt, R. M.; Carroll, P. M.; Brown, K.; Cancilla, M. R.; Chen, C.; de Silva, H.; Franke, Y.; Guan, B.; Heuer, T.; Hung, T.; Keegan, K.; Lee, J. M.; Manne, V.; O'Brien, C.; Parry, D.; Perez-Villar, J. J.; Reddy, R. K.; Xiao, H.; Zhan, H.; Cockett, M.; Plowman, G.; Fitzgerald, K.; Costa, M.; Ross-Macdonald, P. Chemical genetics identifies Rab geranylgeranyl transferase as an apoptotic target of farnesyl transferase inhibitors. *Cancer Cell* **2005**, *7*, 325–336.
- (13) Konstantinopoulos, P. A.; Karamouzis, M. V.; Papavassiliou, A. G. Post-translational modifications and regulation of the RAS superfamily of GTPases as anticancer targets. *Nat. Rev. Drug Discovery* **2007**, *6*, 541–555.
- (14) Karaman, M. W.; Herrgard, S.; Treiber, D. K.; Gallant, P.; Atteridge, C. E.; Campbell, B. T.; Chan, K. W.; Ciceri, P.; Davis, M. I.; Edeen, P. T.; Faraoni, R.; Floyd, M.; Hunt, J. P.; Lockhart, D. J.; Milanov, Z. V.; Morrison, M. J.; Millares, G.; Patel, H. K.; Pritchard, S.; Wodicka, L. M.; Zarrinkar, P. P. A quantitative analysis of kinase inhibitor selectivity. *Nat. Biotechnol.* **2008**, *26*, 127–132.
- (15) Sebti, S. M.; Hamilton, A. D. Farnesyltransferase and geranylgeranyltransferase I inhibitors and cancer therapy: lessons from mechanism and bench-to bedside translational studies. *Oncogene* **2000**, *19*, 6584–6593.
- (16) Gibbs, R. A.; Zahn, T. J.; Sebolt-Leopold, J. S. Nonpeptidic prenyltransferase inhibitors: diverse structural classes and surprising anti-cancer mechanisms. *Curr. Med. Chem.* **2001**, *8*, 1437–1465.
- (17) El Oualid, F.; Cohen, L. H.; van der Marel, G. A.; Overhand, M. Inhibitors of protein: geranylgeranyl transferases. *Curr. Med. Chem.* **2006**, *13*, 2385–2427.
- (18) Bell, I. M. Inhibitors of farnesyltransferase: a rational approach to cancer chemotherapy? *J. Med. Chem.* **2004**, *47*, 1869–1878.
- (19) Baron, R. A.; Tavare, R.; Figueiredo, A. C.; Blazewska, K. M.; Kashemirov, B. A.; McKenna, C. E.; Ebetino, F. H.; Taylor, A.; Rogers, M. J.; Coxon, F. P.; Seabra, M. C. Phosphonocarboxylates inhibit the second geranylgeranyl addition by Rab geranylgeranyl transferase. *J. Biol. Chem.* **2009**, *284*, 6861–6868.
- (20) Coxon, F. P.; Helfrich, M. H.; Van't Hof, R.; Sebti, S.; Ralston, S. H.; Hamilton, A.; Rogers, M. J. Protein geranylgeranylation is required for osteoclast formation, function, and survival: inhibition by bisphosphonates and GGTI-298. *J. Bone Miner. Res.* **2000**, *15*, 1467–1476.
- (21) Coxon, F. P.; Helfrich, M. H.; Larijani, B.; Muzylak, M.; Dunford, J. E.; Marshall, D.; McKinnon, A. D.; Nesbitt, S. A.; Horton, M. A.; Seabra, M. C.; Ebetino, F. H.; Rogers, M. J. Identification of a novel phosphonocarboxylate inhibitor of Rab geranylgeranyl transferase that specifically prevents Rab prenylation in osteoclasts and macrophages. *J. Biol. Chem.* **2001**, *276*, 48213–48222.
- (22) Ren, Z.; Elson, C. E.; Gould, M. N. Inhibition of type I and type II geranylgeranyl-protein transferases by the monoterpene perillyl alcohol in NIH3T3 cells. *Biochem. Pharmacol.* **1997**, *54*, 113–120.
- (23) Castellano, S.; Fiji, H. D. G.; Kinderman, S. S.; Watanabe, M.; de Leon, P.; Tamanoi, F.; Kwon, O. Small-molecule inhibitors of protein geranylgeranyltransferase type I. *J. Am. Chem. Soc.* **2007**, *129*, 5843–5845.
- (24) Watanabe, M.; Fiji, H. D.; Guo, L.; Chan, L.; Kinderman, S. S.; Slamon, D. J.; Kwon, O.; Tamanoi, F. Inhibitors of protein geranylgeranyltransferase I and Rab geranylgeranyltransferase identified from a library of allenoate-derived compounds. *J. Biol. Chem.* **2008**, *283*, 9571–9579.
- (25) Nguyen, U. T.; Guo, Z.; Delon, C.; Wu, Y.; Deraeve, C.; Franzel, B.; Bon, R. S.; Blankenfeldt, W.; Goody, R. S.; Waldmann, H.; Wolters, D.; Alexandrov, K. Analysis of the eukaryotic prenylome by isoprenoid affinity tagging. *Nat. Chem. Biol.* **2009**, *5*, 227–235.
- (26) Wu, Y. W.; Goody, R. S.; Abagyan, R.; Alexandrov, K. Structure of the Disordered C Terminus of Rab7 GTPase Induced by Binding to the Rab Geranylgeranyl Transferase Catalytic Complex Reveals the Mechanism of Rab Prenylation. *J. Biol. Chem.* **2009**, *284*, 13185–13192.
- (27) Breinbauer, R.; Vetter, I. R.; Waldmann, H. From protein domains to drug candidates—natural products as guiding principles in the design and synthesis of compound libraries. *Angew. Chem., Int. Ed.* **2002**, *41*, 2879–2890.
- (28) Newman, D. J.; Cragg, G. M. Natural products as sources of new drugs over the last 25 years. *J. Nat. Prod.* **2007**, *70*, 461–477.
- (29) Omura, S.; Van der Pyl, D.; Inokoshi, J.; Takahashi, Y.; Takeshima, H. Peptidic farnesyl-protein transferase inhibitors produced by an actinomycete. I. Producing strain, fermentation, isolation and biological activity. *J. Antibiot.* **1993**, *46*, 222–228.
- (30) Shiomi, K.; Yang, H.; Inokoshi, J.; Van der Pyl, D.; Nakagawa, A.; Takeshima, H.; Omura, S. Peptidic farnesyl-protein transferase inhibitors produced by an actinomycete. II. Structural elucidation of peptidic farnesyl-protein transferase inhibitors produced by an actinomycete. *J. Antibiot.* **1993**, *46*, 229–34.
- (31) Guo, Z.; Wu, Y. W.; Tan, K. T.; Bon, R. S.; Guiu-Rozas, E.; Delon, C.; Nguyen, T. U.; Wetzel, S.; Arndt, S.; Goody, R. S.; Blankenfeldt, W.; Alexandrov, K.; Waldmann, H. Development of selective RabGGTase inhibitors and crystal structure of a RabGGTase-inhibitor complex. *Angew. Chem., Int. Ed.* **2008**, *47*, 3747–3750.
- (32) Peters, C.; Waldmann, H. Solid-phase synthesis of peptide esters employing the hydrazide linker. *J. Org. Chem.* **2003**, *68*, 6053–6055.
- (33) Kragol, G.; Lumbierres, M.; Palomo, J. M.; Waldmann, H. Solid-phase synthesis of lipidated peptides. *Angew. Chem., Int. Ed.* **2004**, *43*, 5839–5842.
- (34) Lumbierres, M.; Palomo, J. M.; Kragol, G.; Roehrs, S.; Muller, O.; Waldmann, H. Solid-phase synthesis of lipidated peptides. *Chemistry* **2005**, *11*, 7405–7415.
- (35) Stieber, F.; Grether, U.; Waldmann, H. An Oxidation-Labile Traceless Linker for Solid-Phase Synthesis. *Angew. Chem., Int. Ed. Engl.* **1999**, *38*, 1073–1077.
- (36) Stieber, F.; Grether, U.; Waldmann, H. Development of the traceless phenylhydrazide linker for solid-phase synthesis. *Chemistry* **2003**, *9*, 3270–3281.
- (37) Hinterding, K.; Hagenbuch, P.; Rétey, J.; Waldmann, H. Synthesis and In Vitro Evaluation of the Ras Farnesyltransferase Inhibitor Peptidicinnamin E. *Angew. Chem., Int. Ed. Engl.* **1998**, *37*, 1236–1239.
- (38) Thutewohl, M.; Kissau, L.; Popkirova, B.; Karaguni, I. M.; Nowak, T.; Bate, M.; Kuhlmann, J.; Muller, O.; Waldmann, H. Identification of mono- and bisubstrate inhibitors of protein farnesyltransferase and inducers of apoptosis from a peptidicinnamin E library. *Bioorg. Med. Chem.* **2003**, *11*, 2617–2626.
- (39) Thutewohl, M.; Kissau, L.; Popkirova, B.; Karaguni, I. M.; Nowak, T.; Bate, M.; Kuhlmann, J.; Muller, O.; Waldmann, H. Solid-phase synthesis and biological evaluation of a peptidicinnamin E library. *Angew. Chem., Int. Ed.* **2002**, *41*, 3616–20; 3516.
- (40) Thutewohl, M.; Waldmann, H. Solid-phase synthesis of a peptidicinnamin E library. *Bioorg. Med. Chem.* **2003**, *11*, 2591–2615.
- (41) Wu, Y. W.; Alexandrov, K.; Brunsveld, L. Synthesis of a fluorescent analogue of geranylgeranyl pyrophosphate and its use in a high-throughput fluorometric assay for Rab geranylgeranyltransferase. *Nat. Protoc.* **2007**, *2*, 2704–2711.
- (42) Long, S. B.; Casey, P. J.; Beese, L. S. Reaction path of protein farnesyltransferase at atomic resolution. *Nature* **2002**, *419*, 645–650.
- (43) Taylor, J. S.; Reid, T. S.; Terry, K. L.; Casey, P. J.; Beese, L. S. Structure of mammalian protein geranylgeranyltransferase type-I. *EMBO J.* **2003**, *22*, 5963–5974.
- (44) Dursina, B.; Reents, R.; Delon, C.; Wu, Y.; Kulharia, M.; Thutewohl, M.; Veligodsky, A.; Kalinin, A.; Evstifeev, V.; Ciobanu, D.; Szedlaczek, S. E.; Waldmann, H.; Goody, R. S.; Alexandrov, K. Identification and specificity profiling of protein prenyltransferase inhibitors using new fluorescent phosphoisoprenoids. *J. Am. Chem. Soc.* **2006**, *128*, 2822–2835.
- (45) Thoma, N. H.; Iakovenko, A.; Owen, D.; Scheidig, A. S.; Waldmann, H.; Goody, R. S.; Alexandrov, K. Phosphoisoprenoid binding specificity of geranylgeranyltransferase type II. *Biochemistry* **2000**, *39*, 12043–12052.

- (46) Wu, Y. W.; Waldmann, H.; Reents, R.; Ebetino, F. H.; Goody, R. S.; Alexandrov, K. A protein fluorescence amplifier: continuous fluorometric assay for rab geranylgeranyltransferase. *ChemBioChem* **2006**, *7*, 1859–1861.
- (47) Reents, R.; Wagner, M.; Schlummer, S.; Kuhlmann, J.; Waldmann, H. Synthesis and application of fluorescent ras proteins for live-cell imaging. *ChemBioChem* **2005**, *6*, 86–94.
- (48) Kabsch, W. Automatic processing of rotation diffraction data from crystals of initially unknown symmetry and cell constants. *J. Appl. Crystallogr.* **1993**, *26*, 795–800.
- (49) Murshudov, G. N.; Vagin, A. A.; Dodson, E. J. Refinement of macromolecular structures by the maximum-likelihood method. *Acta Crystallogr., Sect. D: Biol. Crystallogr.* **1997**, *53*, 240–255.
- (50) Emsley, P.; Cowtan, K. Coot: model-building tools for molecular graphics. *Acta Crystallogr., Sect. D: Biol. Crystallogr.* **2004**, *60*, 2126–2132.
- (51) Schuttelkopf, A. W.; Van Aalten, D. M. PRODRG: a tool for high-throughput crystallography of protein–ligand complexes. *Acta Crystallogr., Sect. D: Biol. Crystallogr.* **2004**, *60*, 1355–1363.